RSC Advances

PAPER

Published on 27 October 2026
Licensed under CC-BY 4.0

Check for updates

Cite this: *RSC Adv.*, 2026, **16**, 66534

Reducing photosensitizer aggregation *via* cyclodextrin–adamantane porphyrin host–guest interactions for enhanced photodynamic therapy

Chengcheng Liu,[ab] Lijun Yue,[b] Chuning Jia,[b] Yelin Wu *[ab] and Chaochao Wang*[b]

The production yield of singlet oxygen ($^1O_2$) directly determines the therapeutic efficacy of photodynamic therapy (PDT). However, photosensitizer aggregation seriously suppresses $^1O_2$ production. Herein, we developed a host–guest complexation-based isolation strategy that prevents photosensitizers' aggregation, enhances $^1O_2$ generation and ultimately boosts the photodynamic killing performance. Specifically, we synthesized ultra-small $Cu_{2-x}Se$-CD nanoparticles as a supramolecular loading platform and loaded them with adamantane-functionalized 5-(4-hydroxyphenyl)-10,15,20-triphenylporphyrin (Ada-TPP) to obtain a supramolecular nano-photosensitizer $Cu_{2-x}Se$-CD-TPP. In this construct each photosensitizer molecule is individually confined within the cavity of a cyclodextrin unit anchored on the surface of $Cu_{2-x}Se$ nanoparticles, endowing the material with excellent dispersibility and effectively suppressing the photosensitizer's aggregation. This rational structural design results in an 84.8% increase in $^1O_2$ production yield. Both *in vitro* and *in vivo* experiments confirm that $Cu_{2-x}Se$-CD-TPP achieves efficient tumor therapy under light irradiation. Collectively, this study not only provides a robust strategy to mitigate photosensitizers' aggregation, but also develops a promising nanomaterial for precise and high-efficacy photodynamic therapy.

Received 14th June 2026
Accepted 22nd October 2026

DOI: 10.1039/d6ra05237a

rsc.li/rsc-advances

1. Introduction

Photodynamic therapy (PDT) has been widely regarded as an attractive and effective cancer treatment modality in recent decades. It mainly kills tumor cells by utilizing singlet oxygen generated by a photosensitizer under light irradiation.[1,2] Thus, the yield of singlet oxygen directly determines the therapeutic efficacy of PDT. Porphyrin-based photosensitizers are among the most extensively studied and clinically employed photosensitizers for PDT.[3,4] However, porphyrin photosensitizers possess strong hydrophobicity and a large π-conjugated system, which lead to their aggregation in the aqueous physiological environment.[5,6] This aggregation causes photosensitizers to dissipate energy as heat or superoxide anions upon light irradiation, while the quantum yields of $^1O_2$ are significantly reduced.[7,8] Worse, the generated heat is insufficient to raise the temperature of tumor tissues to a lethal level, and the superoxide anions produced are rapidly cleared by high levels of SOD in the tumor microenvironment.[9,10] Therefore, the aggregation of photosensitizers severely impairs singlet oxygen-dependent PDT.

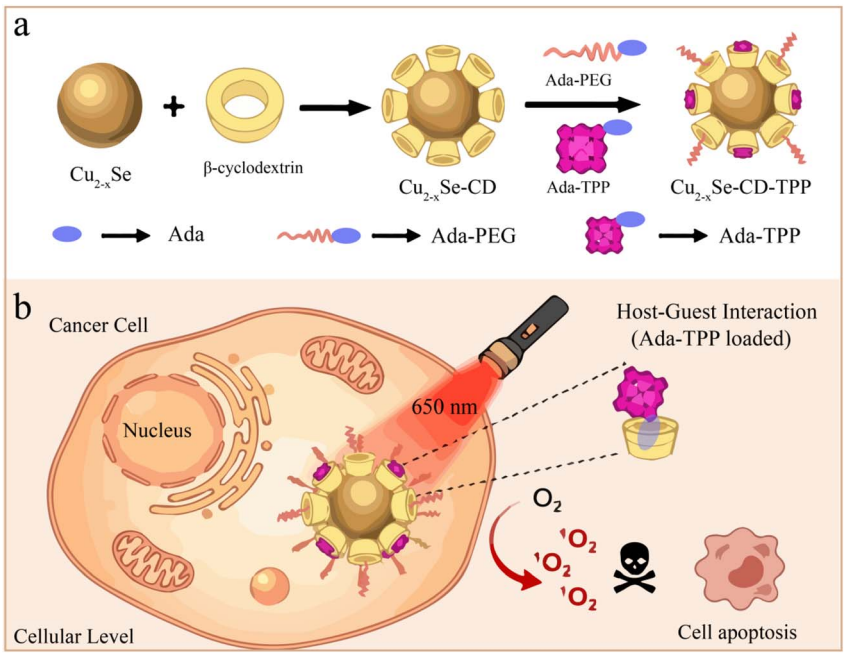
To address the aggregation of porphyrin-based photosensitizers, a variety of strategies have been developed, which generally fall into three categories: improving intrinsic water solubility *via* chemical modification (*e.g.*, grafting hydrophilic components such as glutathione or PEG onto the photosensitizer backbone),[11–13] designing responsive photosensitizers for the tumor microenvironment, and introducing steric barriers to suppress intermolecular aggregation (*e.g.*, constructing POSS–porphyrin alternating copolymers).[14,15] Although these strategies have achieved progress in inhibiting photosensitizer aggregation, they still face notable limitations when applied to many common porphyrin photosensitizers. Major limitations include insufficient steric isolation of photosensitizer molecules, incomplete stimuli-responsiveness, and severe premature leakage during systemic delivery.[16–18] Accordingly, developing general and effective novel strategies to prevent porphyrin photosensitizer aggregation is critically important for advancing the efficacy of PDT.

Cyclodextrins (CDs) are a class of cyclic oligosaccharides, typically consisting of 6–12 D-glucopyranose units. Among them, CDs containing 6, 7, or 8 sugar units are defined as α-, β-, and γ-cyclodextrins, respectively.[19,20] These CDs possess a unique structure: a hydrophobic inner cavity and a hydrophilic outer surface, rendering them water-soluble, which has attracted extensive research attention.[21–23] CDs can be anchored onto

[a]*School of Medicine, Anhui University of Science and Technology, Huainan 232001, P. R. China*

[b]*Institute of Hepatobiliary and Pancreatic Surgery, Department of Hepatobiliary and Pancreatic Surgery, Shanghai East Hospital, School of Medicine, Tongji University, Shanghai, 200120, P. R. China. E-mail: sk_wuyelin@tongji.edu.cn; wcchao@tongji.edu.cn*

© 2026 The Author(s). Published by the Royal Society of Chemistry



Scheme 1 (a) Synthetic route of $Cu_{2-x}Se$-CD-TPP; (b) the anti-tumor process of $Cu_{2-x}Se$-CD-TPP.

nanomaterial surface of nanomaterials to render inherently hydrophobic nanomaterials dispersible in aqueous solution.[24,25] Additionally, the hydrophobic inner cavity of CDs can interact with specific guest molecules *via* host–guest interactions, enabling efficient drug encapsulation.[26] The host–guest complexes formed by CDs and drugs typically exhibit 2 : 1 or 1 : 1 stoichiometries, a feature that allows one or more CD molecules to encapsulate a single drug molecule.[27,28] Among the reported CDs/guest systems, the combination of β-CD and adamantane is the most well-established. The host–guest interaction between β-CD and adamantane is extremely strong, with an association constant of 10^5 M^{-1}, which typically forms 1 : 1 host–guest complexes.[29,30] Therefore, engineering host–guest complexation between porphyrin-based photosensitizers (guests) and CDs offers a strategy to suppress intermolecular interactions between photosensitizers, alleviate aggregation-induced quenching, and ultimately boost PDT efficacy.

Herein, we propose a host–guest complexation-based isolation strategy to inhibit photosensitizer aggregation and enhance photodynamic killing efficacy. Specifically, we synthesized a supramolecular nano-platform $Cu_{2-x}Se$-CD, featuring a core of ultra-small cuprous selenide nanoparticles ($Cu_{2-x}Se$ NPs) surface-modified with mercapto-β-cyclodextrin (HS-β-CD). Then $Cu_{2-x}Se$-CD was employed to load adamantane-functionalized 5-(4-hydroxyphenyl)-10,15,20-triphenylporphyrin (Ada-TPP), yielding the supramolecular nano-photosensitizer $Cu_{2-x}Se$-CD-TPP (Scheme 1). $Cu_{2-x}Se$-CD-TPP exhibited an ultrasmall size of ~4–6 nm and excellent aqueous dispersibility, and compared to free Ada-TPP, $Cu_{2-x}Se$-CD-TPP showed an 84.8% increase of singlet oxygen yield under laser irradiation. Moreover, the supramolecular nano-photosensitizer exhibited excellent photoacoustic imaging capabilities. Ultimately, $Cu_{2-x}Se$-CD-TPP exhibited an excellent therapeutic efficacy of PDT. This study not only provides a new strategy to address the photosensitizer aggregation challenge but also expands the application of host–guest chemistry in tumor treatment.

2. Results and discussion

2.1 Construction of ultra-small supramolecular loading nanoplatform ($Cu_{2-x}Se$-CD)

The fabrication of the ultra-small supramolecular loading nanoplatform $Cu_{2-x}Se$-CD was achieved *via* two key steps. Briefly, non-stoichiometric ultra-small $Cu_{2-x}Se$ nanoparticles were synthesized through $NaBH_4$-mediated reduction of Se powder, followed by the addition of $CuCl_2$.[31,32] As shown in Fig. 1a, the X-ray diffraction (XRD) pattern of the as-synthesized $Cu_{2-x}Se$ matches well with the standard reference (PDF no. 06-0680). A transmission electron microscopy (TEM) image revealed that the synthesized $Cu_{2-x}Se$ nanoparticles have an ultra-small average core size of 2–3 nm (Fig. 1b).

Subsequently, the as-prepared $Cu_{2-x}Se$ nanoparticles were functionalized with mercapto-β-cyclodextrin (HS-β-CD) *via* the strong coordination interaction between thiol groups and copper ions, yielding the final $Cu_{2-x}Se$-CD nanoplatform. As shown in Fig. 1c, thermogravimetric analysis (TGA) revealed that $Cu_{2-x}Se$-CD exhibited substantially higher weight loss than unmodified $Cu_{2-x}Se$ over the temperature range of 200–400 °C. This weight loss is typically attributed to the thermal decomposition of the organic component (HS-β-CD). These results confirm the successful grafting of HS-β-CD onto the surface of $Cu_{2-x}Se$ nanoparticles, and this conclusion is further supported by the observed changes in dynamic light scattering (DLS) size

© 2026 The Author(s). Published by the Royal Society of Chemistry

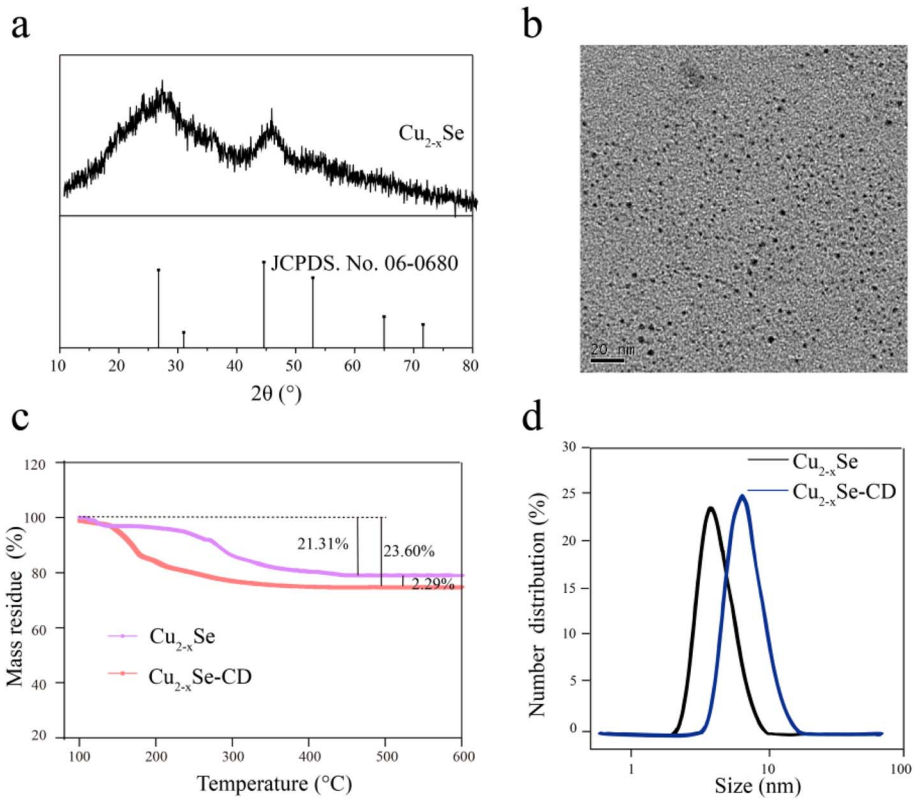


Fig. 1 The construction of $Cu_{2-x}Se$-CD nano-platform. (a) The XRD spectra of $Cu_{2-x}Se$. (b) The TEM image of $Cu_{2-x}Se$. (c) The TGA curves of $Cu_{2-x}Se$ and $Cu_{2-x}Se$-CD. (d) The DLS size of $Cu_{2-x}Se$ and $Cu_{2-x}Se$-CD.

and zeta potential (Fig. 1d and S1). Collectively, the above characterization results verify the successful preparation of the $Cu_{2-x}Se$-CD nanoplatform.

2.2 Preparation of ultra-small supramolecular nano-photosensitizers ($Cu_{2-x}Se$-CD-TPP)

To obtain ultra-small supramolecular nano-photosensitizers ($Cu_{2-x}Se$-CD-TPP), adamantane-functionalized 5-(4-hydroxyphenyl)-10,15,20-triphenylporphyrin (Ada-TPP) was synthesized following previously reported procedures.[33,34] As shown in Fig. 2a, the ^{1}H NMR spectrum of purified Ada-TPP displays characteristic resonances corresponding to the phenylporphyrin moiety: signals at 7.0–9.0 ppm and −2.8 ppm, as well as the characteristic adamantane peaks at 1.5–2.0 ppm. The integral ratio of the two sets of signals was calculated to be 1 : 1, confirming the successful synthesis of Ada-TPP. Subsequently, the host–guest complexation between HS-CD and Ada-TPP was systematically investigated. Obvious chemical-shift perturbations of adamantane protons were detected upon mixing HS-CD with Ada-TPP (Fig. 2b), which is indicative of an altered local chemical microenvironment driven by the insertion of the adamantane group into the cyclodextrin cavity. Fluorescence titration experiments revealed concentration-dependent fluorescence enhancement of Ada-TPP with gradual addition of HS-CD (Fig. 2c). Non-linear regression fitting based on a 1 : 1 host–guest binding model yielded an association constant of $K_a = (2.48 \pm 0.27) \times 10^5\ M^{-1}$ ($R^2 = 0.988$, Fig. S2), further corroborating the efficient host–guest interaction between HS-CD and Ada-TPP, indicating $Cu_{2-x}Se$-CD could load Ada-TPP to prepare $Cu_{2-x}Se$-CD-TPP.

Then, the experiment of $Cu_{2-x}Se$-CD loading Ada-TPP was carried out, and to enhance the dispersibility and biocompatibility of nanomaterial, a synthesized adamantane-functionalized polyethylene glycol (Ada-PEG) was added to the system (Fig. S3). As shown in Fig. 2d, $Cu_{2-x}Se$-CD-PEG and $Cu_{2-x}Se$-CD-TPP exhibited total weight losses of 44.80% and 54.64%, respectively. The increased organic weight loss (9.84%) confirms that Ada-TPP was successfully loaded onto the surface of $Cu_{2-x}Se$-CD to obtain the ultra-small supramolecular nano-photosensitizers $Cu_{2-x}Se$-CD-TPP. To further validate the successful preparation of $Cu_{2-x}Se$-CD-TPP, we also measured the hydrodynamic diameter and zeta potential of both products. As illustrated in Fig. 2e, f and S4a, b, $Cu_{2-x}Se$-CD-TPP exhibited favorable stability, while showing distinct physicochemical changes relative to $Cu_{2-x}Se$-CD, confirming successful Ada-TPP loading. Meanwhile, TEM imaging of $Cu_{2-x}Se$-CD-TPP (Fig. 2g) revealed a particle size of 4–6 nm, which was significantly larger than that of $Cu_{2-x}Se$-CD. Additionally, X-ray diffraction (XRD) patterns verified that the as-synthesized $Cu_{2-x}Se$-CD-TPP was highly consistent with the standard reference (PDF no. 06-0680), and its crystal structure remained stable compared with pure $Cu_{2-x}Se$ (Fig. S5). The Ada-TPP loading content was determined to be 10.39 ± 0.42 wt% from the standard curve built upon its Soret-band absorbance at 414 nm (Fig. S6a and b), which is in

© 2026 The Author(s). Published by the Royal Society of Chemistry

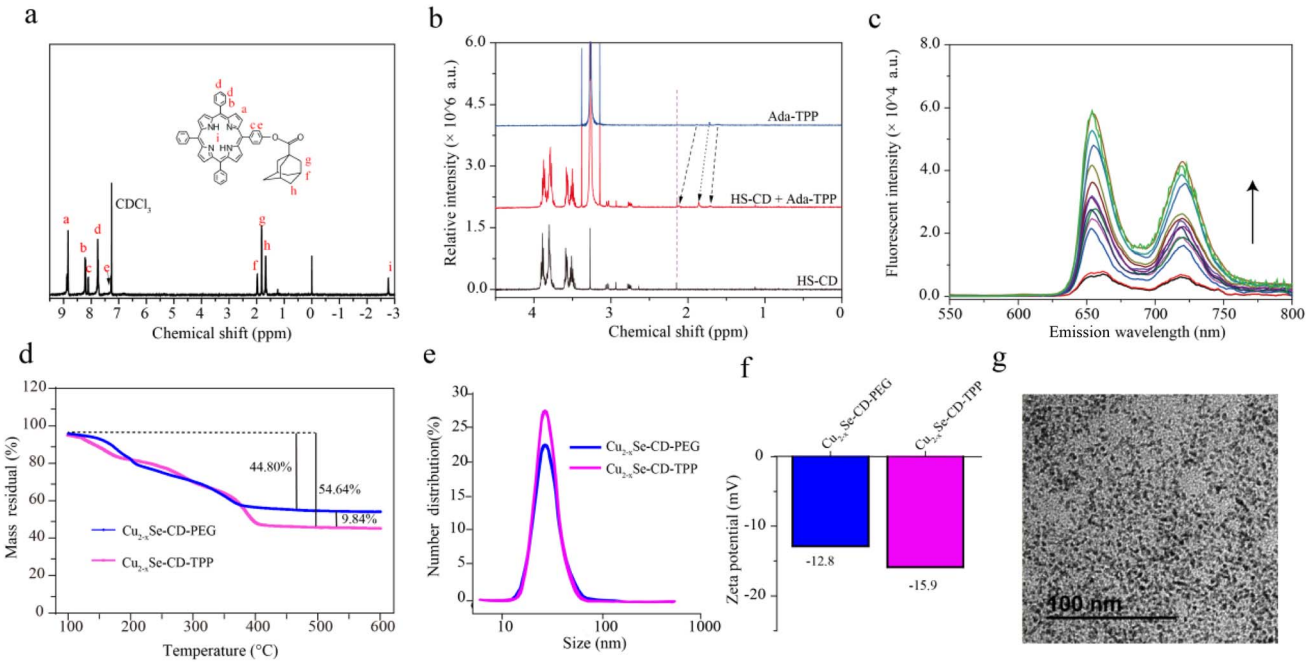


Fig. 2 The preparation of $Cu_{2-x}Se$-CD-TPP nano-photosensitizers (a) the ^1H NMR spectrum of Ada-TPP. (b) ^1H NMR spectra of free HS-CD, free Ada-TPP, and HS-CD + Ada-TPP mixture. (c) Fluorescence spectra of Ada-TPP (1.0×10^{-5} M) in aqueous solution with different concentrations of HS-CD: 0, 0.2, 0.4, 0.6, 0.8, 1.5, 3.0, 4.0, 6.0, 8.0, 10.0, and 12.0×10^{-5} M. (d) The TGA curves of $Cu_{2-x}Se$-CD-PEG and $Cu_{2-x}Se$-CD-TPP. (e) The DLS size of $Cu_{2-x}Se$-CD-PEG and $Cu_{2-x}Se$-CD-TPP. (f) The zeta potential of $Cu_{2-x}Se$-CD-PEG and $Cu_{2-x}Se$-CD-TPP. (g) The TEM image of $Cu_{2-x}Se$-CD-TPP.

good agreement with the weight-loss value obtained from TGA measurements. Collectively, these results confirm the successful synthesis of ultra-small supramolecular nano-photosensitizers $Cu_{2-x}Se$-CD-TPP.

2.3 Evaluation of Ada-TPP aggregation in $Cu_{2-x}Se$-CD-TPP

To verify that the host–guest complexation between HS-CD and Ada-TPP could suppress porphyrin aggregation, a series of spectroscopic experiments were performed. As shown in Fig. 3a, Ada-TPP and OH-TPP exhibited a sharp Soret band in methanol, but in aqueous solution, obvious broadening and decreased absorbance of the Soret band were observed, indicating severe aggregation of Ada-TPP and OH-TPP in water. In addition, consistent with aggregation-induced quenching, Ada-TPP and OH-TPP in water displayed heavily suppressed fluorescence emission (Fig. S7). However, it is obvious that $Cu_{2-x}Se$-CD-TPP obtained *via* host–guest assembly exhibited well-defined sharp Soret band (Fig. 3b) and $Cu_{2-x}Se$-CD-TPP displayed strong fluorescence emission (Fig. 3c). These observations demonstrate that the host–guest complexation between HS-CD and Ada-TPP effectively alleviated porphyrin aggregation.

To further verify this point, the time-resolved fluorescence decay and absolute fluorescence quantum yields were also measured. As shown in Fig. 3d and e, free aqueous Ada-TPP possessed a low quantum yield of 6.5%, whereas $Cu_{2-x}Se$-CD-TPP afforded a much higher quantum yield of 19.3%. In addition, compared with the fluorescence lifetime of Ada-TPP (3.20 ns), that in $Cu_{2-x}Se$-CD-TPP (4.2 ns) has been significantly prolonged. All these results indicated that cyclodextrin-adamantane host–guest interaction suppressed non-radiative decay pathways originating from porphyrin intermolecular aggregation.

2.4 Evaluation of ROS generation and photoacoustic imaging capabilities of $Cu_{2-x}Se$-CD-TPP

To evaluate the singlet oxygen ($^1O_2$) generation capability of $Cu_{2-x}Se$-CD-TPP, a 1,3-diphenylbenzofuran (DPBF) degradation assay was performed. As illustrated in Fig. 4a and S8, negligible DPBF degradation was detected for the light-only or $Cu_{2-x}Se$-CD + light groups. By contrast, both the Ada-TPP and $Cu_{2-x}Se$-CD-TPP groups exhibited pronounced DPBF degradation upon light exposure. Notably, the $Cu_{2-x}Se$-CD-TPP group displayed substantially faster degradation kinetics than the Ada-TPP group (Fig. 4b and c). These results confirm that both $Cu_{2-x}Se$-CD-TPP and Ada-TPP can generate $^1O_2$ under light irradiation, and $Cu_{2-x}Se$-CD-TPP affords a higher $^1O_2$ yield than free Ada-TPP. Furthermore, by comparing the DPBF degradation slopes, we obtained a slope of −0.7317 for Ada-TPP and −1.3220 for $Cu_{2-x}Se$-CD-TPP (Fig. 4d), corresponding to an 84.8% increase in $^1O_2$ yield for $Cu_{2-x}Se$-CD-TPP relative to the free photosensitizer control. This improvement in $^1O_2$ production is ascribed to the spatial separation of porphyrin photosensitizers on the $Cu_{2-x}Se$-CD ultra-small supramolecular nanoplatform mediated by cyclodextrin, which effectively alleviates aggregation-caused quenching (ACQ).

© 2026 The Author(s). Published by the Royal Society of Chemistry

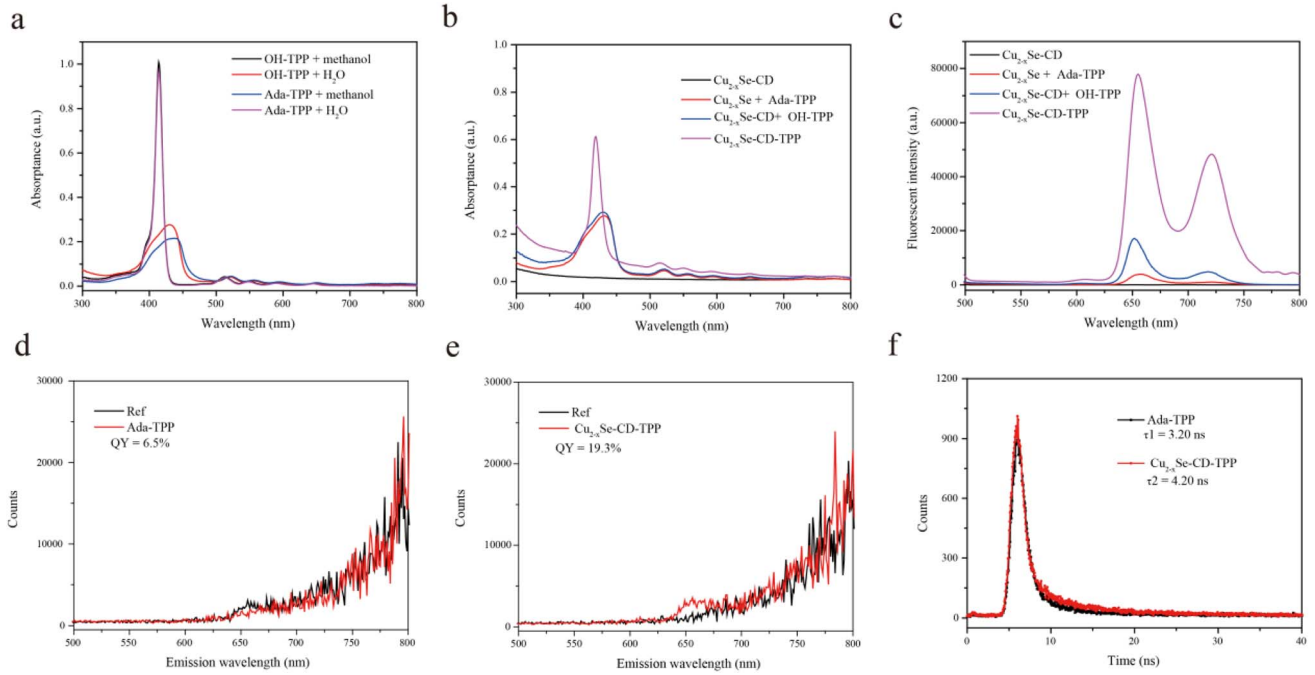


Fig. 3 Spectroscopic characterizations of Ada-TPP and $Cu_{2-x}Se$-CD-TPP. (a) UV-Vis absorption spectra of Ada-TPP in water and methanol. (b) UV-vis absorption spectra of $Cu_{2-x}Se$-CD, $Cu_{2-x}Se$ + TPP, $Cu_{2-x}Se$ + OH-TPP and $Cu_{2-x}Se$-CD-TPP. (c) Fluorescence emission spectra of different nanocomposites. (d and e) Absolute fluorescence quantum yields of Ada-TPP and $Cu_{2-x}Se$-CD-TPP. (f) Fluorescence lifetime decay curves of $Cu_{2-x}Se$-CD-TPP and free Ada-TPP measured by an integrating sphere.

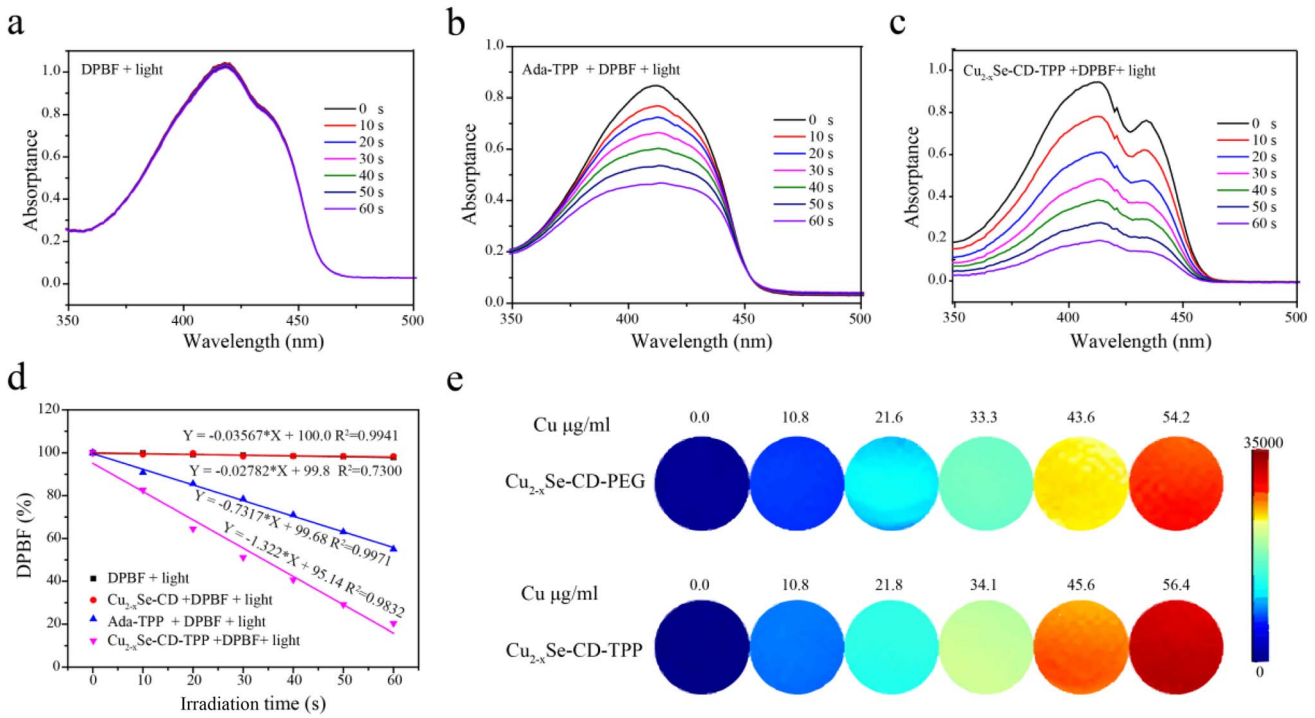


Fig. 4 The ROS generation and photoacoustic imaging capabilities of $Cu_{2-x}Se$-CD-TPP *in vitro*. (a–c) The UV-Vis absorptance spectra of DPBF in different groups with light irradiation (blank, Ada-TPP and $Cu_{2-x}Se$-CD-TPP). (d) The relative UV-Vis absorptance of DPBF at 420 nm with light irradiation time (blank, $Cu_{2-x}Se$-CD, Ada-TPP and $Cu_{2-x}Se$-CD-TPP). (e) To investigate the photoacoustic imaging (PAI) properties of $Cu_{2-x}Se$-CD-PEG and $Cu_{2-x}Se$-CD-TPP at various concentrations under 808 nm laser irradiation, as well as the relationship between their concentrations and PAI performance.

© 2026 The Author(s). Published by the Royal Society of Chemistry

Additionally, the photoacoustic (PA) imaging performance of $Cu_{2-x}Se$-CD-TPP was evaluated. As illustrated in Fig. 4e, the PA signals of $Cu_{2-x}Se$-CD-PEG and $Cu_{2-x}Se$-CD-TPP at 808 nm were clearly enhanced with increasing concentrations. Further linear regression analysis (Fig. S9) demonstrated a strong linear correlation between the PA signal intensity and concentration for both samples. Collectively, these findings indicate that $Cu_{2-x}Se$-CD-TPP can serve as an effective PA imaging agent for real-time monitoring of its *in vivo* distribution, thereby providing reliable guidance for subsequent PDT.

2.5 Evaluation of the cell-killing performance of $Cu_{2-x}Se$-CD-TPP

Firstly, cellular internalization of $Cu_{2-x}Se$-CD-TPP by 4T1 cells was verified *via* confocal laser scanning microscopy (CLSM). As shown in Fig. 5a, porphyrin red fluorescence was evident within 4T1 cells, with the signal intensity increasing as incubation time prolonged. Together, these observations confirm that 4T1 cells internalize $Cu_{2-x}Se$-CD-TPP in a time-dependent manner. Following confirmation of cellular internalization, intracellular reactive oxygen species (ROS) generation by $Cu_{2-x}Se$-CD-TPP under light irradiation was assessed using the ROS-sensitive probe DCFH-DA. As shown in Fig. 5b, negligible fluorescence was detected in the groups treated with laser alone or $Cu_{2-x}Se$-

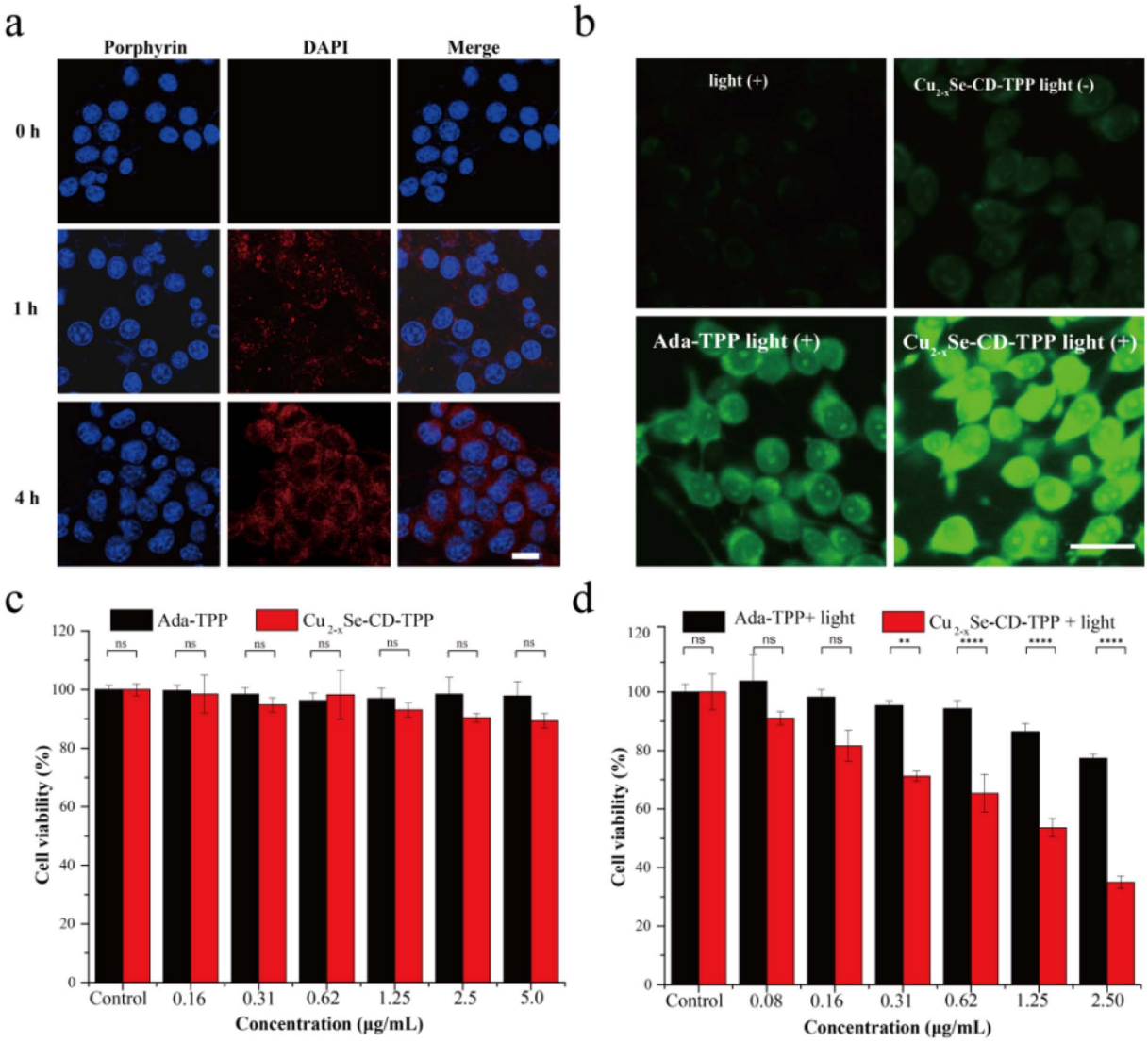


Fig. 5 The cytotoxicity of $Cu_{2-x}Se$-CD-TPP to 4T1 cells with/without light irradiation. (a) The confocal images of 4T1 cells cultured with $Cu_{2-x}Se$-CD-TPP for 1 h and 4 h (scale bar, 20 μm). (b) Confocal images of detection for ROS in 4T1 cells with DCFH (scale bar, 20 μm). (c) The cell viability of Ada-TPP and $Cu_{2-x}Se$-CD-TPP to 4T1 cells under dark conditions. (d) The cell viability of Ada-TPP and $Cu_{2-x}Se$-CD-TPP to 4T1 cells with light irradiation (650 nm laser, 0.5 W cm^{-2}). Data are presented with $n = 6$ technical replicates per group. Statistical comparisons were performed using two-way analysis of variance (ANOVA) followed by Tukey's honestly significant difference (HSD) *post hoc* test for multiple comparisons between concentration groups (ns: not significant, $^{**}p < 0.01$, $^{****}p < 0.0001$).

© 2026 The Author(s). Published by the Royal Society of Chemistry

CD-TPP alone. By comparison, robust green fluorescence was observed in cells treated with Cu_{2-x}Se-CD-TPP plus light, with the fluorescence intensity significantly higher in the Cu_{2-x}Se-CD-TPP group than that in the Ada-TPP group. The results revealed that Cu_{2-x}Se-CD-TPP generated higher levels of ROS than Ada-TPP upon 650 nm laser excitation with equal porphyrin concentrations.

Building on these ROS generation results, the killing efficacy of Cu_{2-x}Se-CD-TPP to tumor cells was assessed using the MTT assay. As presented in Fig. 5c and S10, 4T1 cells treated with Ada-TPP or Cu_{2-x}Se-CD-TPP retained cell viability over 90% at porphyrin concentrations up to 5.0 μg mL^{-1} in the dark. This result confirms the excellent biocompatibility of Cu_{2-x}Se-CD-TPP without laser irradiation. However, upon 650 nm laser irradiation (0.5 W cm^{-2}, 5 min), Cu_{2-x}Se-CD did not exhibit cytotoxicity at the same copper concentration as Cu_{2-x}Se-CD-TPP (Fig. S11), and both Ada-TPP and Cu_{2-x}Se-CD-TPP exerted evident concentration-dependent cytotoxicity toward 4T1 cells (Fig. 5d). Under the same porphyrin content and irradiation parameters, Cu_{2-x}Se-CD-TPP showed markedly stronger cytotoxicity than Ada-TPP, and produced prominent cell inhibition even at a low porphyrin concentration of 0.16 μg mL^{-1}. Collectively, these findings confirm that host–guest interactions suppress the aggregation of porphyrin photosensitizers and further improve their tumor cell killing efficiency.

2.6 Evaluation of the anti-tumor effect of Cu_{2-x}Se-CD-TPP *in vivo*

We next investigated the *in vivo* antitumor efficacy of Cu_{2-x}Se-CD-TPP using 4T1 xenograft mouse models. As shown in Fig. 6a and b, tumor growth curves and representative photographs of 4T1 tumor-xenografted Balb/c mice after treatments showed rapid tumor growth in the blank, light-only and Cu_{2-x}Se-CD-TPP-only groups. By contrast, both the Ada-TPP + light and Cu_{2-x}Se-CD-TPP + light treatments exerted antitumor effects, with the latter producing the most potent tumor inhibition. This trend was further validated by the weights and representative photographs of dissected tumors (Fig. 6c and S12). In addition, mouse body weights remained steady in all groups with no drastic loss (Fig. 6d), demonstrating the good biocompatibility of Cu_{2-x}Se-CD-TPP.

To further prove the efficacy of Cu_{2-x}Se-CD-TPP under light irradiation, tumor cell apoptosis after treatment was evaluated

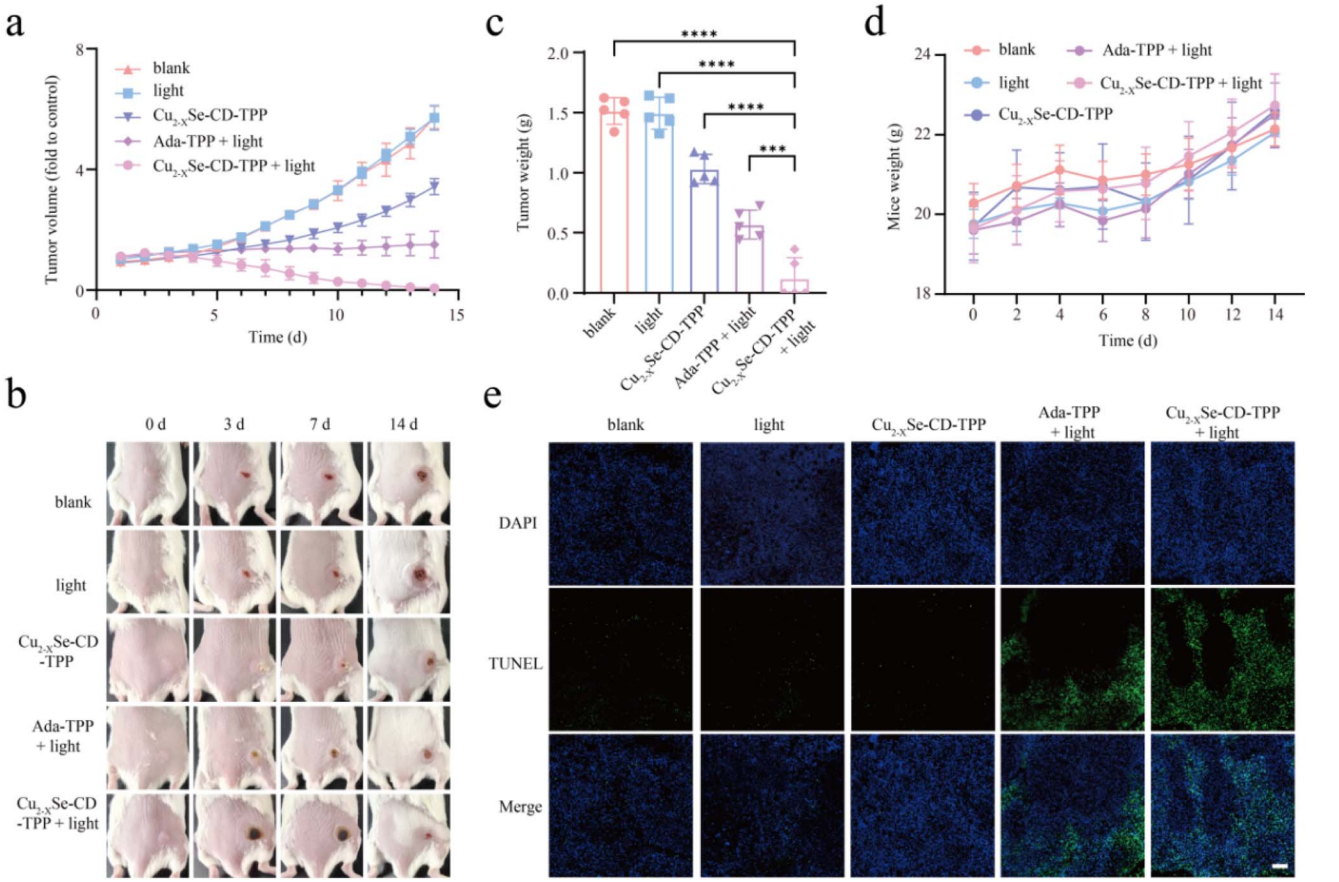


Fig. 6 The anti-tumor performance of Cu_{2-x}Se-CD-TPP *in vivo*. (a) Tumor growth curves of mice after treatments. (b) Representative photographs of 4T1 tumor-xenografted balb/c mice after treatments. (c) Weight of isolated tumors. (d) Body weights of tumor-bearing mice of five groups of mice. (e) TUNEL staining of tumors sections at 48 h after treatments (scale bars: 200 μm). Statistical comparisons were performed using one-way analysis of variance (ANOVA) followed by Tukey's honestly significant difference (HSD) *post hoc* test for multiple comparisons between concentration groups (***$p < 0.001$, and ****$p < 0.0001$).

© 2026 The Author(s). Published by the Royal Society of Chemistry

via TUNEL staining (Fig. 6e). Nearly no apoptotic signals were observed in the blank, light-only, and Cu_{2-x}Se-CD-TPP-only groups. In comparison, positive TUNEL staining was detected in the two combined treatment groups (Ada-TPP + light group and Cu_{2-x}Se-CD-TPP + light group), and the Cu_{2-x}Se-CD-TPP + light group exhibited the highest abundance of apoptotic cells. Additionally, we also observed the temperature elevation upon laser irradiation and it was insufficient to induce tumor ablation (Fig. S13 and S14). These results indicate that Cu_{2-x}Se-CD-TPP upon light irradiation can effectively induce extensive tumor cell apoptosis, accounting for its superior anticancer performance. Overall, these findings proved that host–guest interactions inhibit the aggregation of porphyrin photosensitizers and consequently improve anti-tumor capability.

3. Conclusion

In this study, we provided a host–guest complexation-based isolation strategy to suppress porphyrin photosensitizer aggregation and improve the therapeutic efficacy of PDT. Starting from ultra-small Cu_{2-x}Se nanoparticles and mercapto-β-cyclodextrin, we constructed the Cu_{2-x}Se-CD supramolecular nanoplatform, which was then loaded with adamantane-functionalized porphyrin photosensitizer to afford the ultra-small Cu_{2-x}Se-CD-TPP supramolecular nano-photosensitizer with an Ada-TPP loading content of ∼10.39 wt%. The fluorescence titration of the molecular HS-CD/Ada-TPP model system supports a host–guest association, while the spectroscopic characterization of the nanoparticle assembly is consistent with spatial isolation of Ada-TPP, which effectively prevents porphyrin photosensitizers' aggregation. Compared to free photosensitizer, Cu_{2-x}Se-CD-TPP exhibited an 84.8% increase in $^1O_2$ production yield and achieved efficient tumor cell killing. In addition, Cu_{2-x}Se-CD-TPP displayed an excellent anti-tumor performance. Overall, this work not only developed a novel strategy to prevent photosensitizer aggregation, but also develops a promising nanomaterial for high-efficacy PDT.

Ethical statement

All animal procedures were performed in accordance with the Guidelines for Care and Use of Laboratory Animals of Tongji University and experiments were approved by the Animal Ethics Committee of Tongji University (Approval Number: TJ-HB-LAC-202305).

Author contributions

Y. W. and C. W., conceived and designed the research. C. L., C. W., and L. Y. performed the related experiments and prepared the nanomaterials. C. L. and C. J. evaluated the functions of nanomaterials *in vitro* and *in vivo*. C. L., and C. W. arranged and analyzed the data. C. L., and C. W. wrote the manuscript. C. L., C. W., and Y. W. revised the paper. All authors contributed to the discussion results and commented on the manuscript.

Conflicts of interest

The authors declare no competing interests.

Data availability

All supporting data generated and analysed in this study are included within the article and the accompanying supplementary information (SI). The raw experimental data that support the findings of this work are available from the corresponding author upon reasonable request. Supplementary information is available. See DOI: https://doi.org/10.1039/d6ra05237a.

Acknowledgements

This work was generously supported by the National Natural Science Foundation of China (Grant No. U25A20245, 82202304), and the Medical Discipline Construction Program of Shanghai Pudong New Area Health Commission (PWXx2025-03).

References

1 S. S. Lucky, K. C. Soo and Y. Zhang, Nanoparticles in photodynamic therapy, *Chem. Rev.*, 2015, **115**(4), 1990–2042.
2 X. Li, S. Lee and J. Yoon, Supramolecular photosensitizers rejuvenate photodynamic therapy, *Chem. Soc. Rev.*, 2018, **47**(4), 1174–1188.
3 A. Akbar, S. Khan, T. Chatterjee, *et al.*, Unleashing the power of porphyrin photosensitizers: Illuminating breakthroughs in photodynamic therapy, *J. Photochem. Photobiol., B*, 2023, **248**, 112796.
4 W. Zhao, L. Wang, M. Zhang, *et al.*, Photodynamic therapy for cancer: mechanisms, photosensitizers, nanocarriers, and clinical studies, *MedComm*, 2024, **5**, e603.
5 C. Qi, J. Chen, Y. Qu, *et al.*, Recent Advances in Porphyrin-Based Covalent Organic Frameworks for Synergistic Photodynamic and Photothermal Therapy, *Pharmaceutics*, 2024, **16**(12), 1625.
6 Y. Ohishi, T. Ichikawa, S. Yokoyama, *et al.*, Water-Soluble Rotaxane-Type Porphyrin Dyes as a Highly Membrane-Permeable and Durable Photosensitizer Suitable for Photodynamic Therapy, *ACS Appl. Bio Mater.*, 2024, **7**(10), 6656–6664.
7 Z. Zhuang, J. Li, P. Shen, *et al.*, Exploring and leveraging aggregation effects on reactive oxygen species generation in photodynamic therapy, *Aggregate*, 2024, **5**, e540.
8 J. Ni, Y. Wang, H. Zhang, *et al.*, Aggregation-Induced Generation of Reactive Oxygen Species: Mechanism and Photosensitizer Construction, *Molecules*, 2021, **26**(2), 268.
9 Y. Shang, X. Yi, D. Xiang, *et al.*, Nanoagent-Mediated Photothermal Therapy: From Delivery System Design to Synergistic Theranostic Applications, *Int. J. Nanomed.*, 2025, **20**, 6891–6927.
10 G. Szewczyk and K. Mokrzyński, Concentration-Dependent Photoproduction of Singlet Oxygen by Common Photosensitizers, *Molecules*, 2025, **30**(5), 1130.

© 2026 The Author(s). Published by the Royal Society of Chemistry

11 P. Kumari, M. Paul, H. Bhatt, *et al.*, Chlorin e6 Conjugated Methoxy-Poly(Ethylene Glycol)-Poly(D,L-Lactide) Glutathione Sensitive Micelles for Photodynamic Therapy, *Pharm. Res.*, 2020, **37**(2), 18.
12 K. Xu, T. Zhang, J. Shao, *et al.*, Research progress in glutathione-responsive photosensitizers for tumor therapy, *Chin. J. Lasers*, 2023, **50**(3), 0307202.
13 C. Wang, L. Liu, H. Cao, *et al.*, Intracellular GSH-activated galactoside photosensitizers for targeted photodynamic therapy and chemotherapy, *Biomater. Sci.*, 2017, **5**(2), 274–284.
14 J. Jin, Y. Zhu, Z. Zhang, *et al.*, Enhancing the Efficacy of Photodynamic Therapy through a Porphyrin/POSS Alternating Copolymer, *Angew Chem. Int. Ed. Engl.*, 2018, **57**(50), 16354–16358.
15 P. Loman-Cortes, T. Binte Huq and J. L. Vivero-Escoto, Use of Polyhedral Oligomeric Silsesquioxane (POSS) in Drug Delivery, Photodynamic Therapy and Bioimaging, *Molecules*, 2021, **26**(21), 6453.
16 D. Lee, S. Kwon, S. Y. Jang, *et al.*, Overcoming the obstacles of current photodynamic therapy in tumors using nanoparticles, *Bioact. Mater.*, 2021, **8**, 20–34.
17 X. Wu, Y. Chen, Q. Guo, *et al.*, Cyclodextrin-Based Nanoplatforms for Tumor Phototherapy: An Update, *Pharmaceutics*, 2022, **14**(7), 1375.
18 M. Tang, Y. Song, Y. L. Lu, *et al.*, Cyclodextrin-Activated Porphyrin Photosensitization for Boosting Self-Cleavable Drug Release, *J. Med. Chem.*, 2022, **65**(9), 6764–6774.
19 I. Spiridon and N. Anghel, Cyclodextrins as Multifunctional Platforms in Drug Delivery and Beyond: Structural Features, Functional Applications, and Future Trends, *Molecules*, 2025, **30**(14), 3044.
20 T. Loftsson and M. E. Brewster, Pharmaceutical applications of cyclodextrins. 1. Drug solubilization and stabilization, *J. Pharm. Sci.*, 1996, **85**(10), 1017–1025.
21 B. G. Poulson, Q. A. Alsulami, A. Sharfalddin, *et al.*, Cyclodextrins: Structural, Chemical, and Physical Properties, and Applications, *Polysaccharides*, 2022, **3**(1), 1–31.
22 P. Jansook, N. Ogawa and T. Loftsson, Cyclodextrins: structure, physicochemical properties and pharmaceutical applications, *Int. J. Pharm.*, 2018, **535**(1–2), 272–284.
23 B. Tian, S. Hua and J. Liu, Cyclodextrin-based delivery systems for chemotherapeutic anticancer drugs: A review, *Carbohydr. Polym.*, 2020, **232**, 115805.
24 Q. Zhang, C. Shen, N. Zhao, *et al.*, Redox-responsive and drug-embedded silica nanoparticles with unique self-destruction features for efficient gene/drug codelivery, *Adv. Funct. Mater.*, 2017, **27**(12), 1606229.
25 J. Xu, J. Li, S. Lin, *et al.*, Nanocarrier-Mediated Codelivery of Small Molecular Drugs and siRNA to Enhance Chondrogenic Differentiation and Suppress Hypertrophy of Human Mesenchymal Stem Cells, *Adv. Funct. Mater.*, 2016, **26**(15), 2463–2472.
26 A. M. Musuc, Cyclodextrins: Advances in Chemistry, Toxicology, and Multifaceted Applications, *Molecules*, 2024, **29**(22), 5319.
27 P. Saokham and T. Loftsson, Stoichiometry of cyclodextrin–drug complexes: 1:1, 2:1 and higher-order complexes, *Int. J. Mol. Sci.*, 2024, **25**(9), 4721.
28 P. Saokham, C. Muankaew, P. Jansook, *et al.*, Solubility of Cyclodextrins and Drug/Cyclodextrin Complexes, *Molecules*, 2018, **23**(5), 1161.
29 L. Zhang, J. Li and H. Wang, Supramolecular Engineering of β-Cyclodextrin/Adamantane-Based Nanostructures for Biomedical Applications, *Molecules*, 2026, **31**(7), 584.
30 A. Harada, Cyclodextrin-based molecular machines, *Acc. Chem. Res.*, 2001, **34**(6), 456–464.
31 W. Zhang, X. Zhang, L. Zhang, *et al.*, A redox reaction to synthesize nanocrystalline $Cu_{2-x}Se$ in aqueous solution, *Inorg. Chem.*, 2000, **39**(9), 2268–2270.
32 J. Shim, J. S. Hahn, S. H. Lee, *et al.*, Synthesis and characterization of CIS nanoparticle ink for low-cost thin film solar cells, *J. Nanosci. Nanotechnol.*, 2014, **14**(12), 9279–9284.
33 L. Xia, J. Wu, B. Huang, *et al.*, Enhanced photodynamic therapy through supramolecular photosensitizers with an adamantyl-functionalized porphyrin and a cyclodextrin dimer, *Chem. Commun.*, 2020, **56**(75), 11134–11137.
34 J. Zhou, K. Huang, S. Lin, *et al.*, Supramolecular polymeric micelles self-assembled from adamantane-functionalized porphyrin and β-cyclodextrin polymer for photodynamic therapy, *J. Mater. Chem. B*, 2017, **5**(27), 5846–5853.

© 2026 The Author(s). Published by the Royal Society of Chemistry